CKAP5 deficiency induces premature ovarian insufficiency

Zihao Hu,[a,b] Jingping Gao,[a] Panpan Long,[b] Ruping Quan,[b] Fei Huang,[a] Jixuan Jiang,[a] Jing Zhang,[a] Jianlin Chen,[a,***] Hongmei Xiao,[b,**] and Hualin Huang[a,*]

[a]Reproductive Medicine Center, Department of Obstetrics and Gynecology, The Second Xiangya Hospital, Central South University, Changsha, Hunan, China
[b]Institute of Reproductive & Stem Cell Engineering, School of Basic Medical Science, Central South University, Changsha, Hunan, China

eBioMedicine
2025;115: 105718
Published Online xxx
https://doi.org/10.1016/j.ebiom.2025.105718

Summary

Background Premature ovarian insufficiency (POI) is characterized by ovarian dysfunction that develops from diminished ovarian reserve (DOR). The exact aetiology of POI remains poorly understood. This study aims to elucidate the role of *CKAP5* in the regulation of ovarian function and fertility.

Methods Bulk RNA sequencing of granulosa cells was conducted in the control group and in the patients with DOR to screen for candidate genes, which were further validated by gene burden analysis in a next-generation sequencing cohort of POI and control individuals. Additionally, ovarian reserve was evaluated in heterozygous *Ckap5* knockout mice, alongside the ovarian and oocyte single-cell transcriptome analysis. The regulatory mechanism of CKAP5 was studied through in vivo and in vitro experiments.

Findings *CKAP5* was identified as a key hub gene associated with ovarian ageing. Heterozygous *Ckap5* knockout mice exhibited a POI-like phenotype, characterized by a reduced primordial follicle pool and accelerated follicular atresia. CKAP5 promotes autophagy via ATG7 and simultaneously supports DNA damage repair through the ATM. Finally, a variant in *CKAP5* (NM_0001008938.4, c.630 + 7_630 + 11delCAAAA) was identified in patients with POI, resulting in protein truncation and loss of function.

Interpretation CKAP5 deficiency induces premature ovarian insufficiency in both humans and mice.

Funding The National Key R&D Program of China (2017YFC1001100), the National Natural Science Foundation of China (81501248, 81471453 and 81801295), the Health Research Project of Hunan Provincial Health Commission (W20243018), the Science and Technology Innovation Program of Hunan Province (2021RC3031), the National Natural Science Foundation of Hunan Province (2022JJ30066), the Scientific Research Program of Hunan Provincial Health Commission (202205033471 and 21B0058), the Open Research Fund of Hunan Provincial Key Laboratory of Regional Hereditary Birth Defects Prevention and Control (HPKL2023013).

Keywords: CKAP5; Premature ovary insufficiency; DNA damage repair; Autophagy; Apoptosis

Introduction

Premature ovarian insufficiency (POI), also known as Premature ovarian failure (POF), is characterized by primary or secondary amenorrhoea that occurs before the age of 40, with a follicle-stimulating hormone (FSH) levels >25 IU/l on two occasions 4 weeks apart.[1] Recent meta-analyses suggest that the global prevalence of POI is as high as 3.7%.[2] POI significantly threatens both the physiological and psychological health of women. Clinically, patients with POI exhibit reduced ovarian follicles and decreased oestrogen secretion, impairing fertility and leading to long-term complications such as osteoporosis, fractures, cardiovascular diseases, and depression.[3] A decline in ovarian reserve may result from a reduction in the pool of primordial follicles, follicular dysfunction, or the premature depletion of immature follicles due to accelerated atresia.[4] The aetiology of POI is multifactorial, involving genetic,

*Corresponding author. Reproductive Medicine Center, Department of Obstetrics and Gynecology, The Second Xiangya Hospital, Central South University, No.139, Renmin Middle Road, Changsha, Hunan, China.
**Corresponding author. Institute of Reproductive & Stem Cell Engineering, School of Basic Medical Science, Central South University, 88 Xiangya Road, Changsha, Hunan, China.
***Corresponding author. Reproductive Medicine Center, Department of Obstetrics and Gynecology, The Second Xiangya Hospital, Central South University, No.139, Renmin Middle Road, Changsha, Hunan, China.
E-mail addresses: huanghualin@csu.edu.cn (H. Huang), hmxiao@csu.edu.cn (H. Xiao), jianlinchen@csu.edu.cn (J. Chen).

Research in context

Evidence before this study

As a microtubule regulator, CKAP5 has been well-established to promote spindle formation and chromosome segregation during mitosis and meiosis. In vitro, CKAP5 depletion leads to abnormal oocyte nuclear maturation in humans and mice. However, the role of *CKAP5* in ovarian reserve and the onset of premature ovarian insufficiency remains unclear.

Added value of this study

In the present study, we identified an association between *CKAP5* expression deficiency and reduced ovarian function, suggesting *CKAP5* as a gene involved in the regulation of ovarian ageing. *Ckap5* heterozygous mice exhibited a subfertility phenotype, with a reduced ovarian primordial follicle pool and accelerated follicular atresia. CKAP5 deficiency impaired ovarian DNA damage repair and autophagy, leading to increased follicular apoptosis, reduced oocyte quantity, and compromised oocyte quality. ATM and ATG7 serve as key targets that are regulated by CKAP5 in the DNA damage repair and autophagy pathways. Moreover, a loss-of-function variant in *CKAP5* is responsible for clinical premature ovarian insufficiency.

Implications of all the available evidence

These findings demonstrated that CKAP5 maintains ovarian reserve and fertility by promoting autophagy and DNA damage repair. This study provided insights into the genetic causes of premature ovarian insufficiency.

autoimmune, infectious, or iatrogenic factors, with genetic causes accounting for approximately 20%–25% of POI cases.[5] Despite the identification of numerous candidate genes having been identified, the genetic heterogeneity of POI suggests that the aetiology remains unclear in more than half of the cases.

Cytoskeleton-associated protein 5 (*CKAP5*) gene encodes a microtubule-associated protein that belongs to the TOG/XMAP215 family. CKAP5 consists of TOG domains 1–5 and is highly conserved across organisms, including mammals, plants, and yeast. As a microtubule regulator, CKAP5 fulfils multiple roles, including (1) promoting microtubule nucleation and elongation[6,7]; (2) maintaining the centrosome integrity and participating in spindle formation[8]; (3) binding to chromosomal kinetochores to regulate chromosome segregation during mitosis[9]; (4) Constituting the oocyte microtubule organizing centre (MTOC) during human oocyte meiosis.[10] CKAP5 is highly expressed in the ovaries of perinatal mice.[11–13] In vitro depletion of CKAP5 through microinjection results in abnormal nuclear maturation in oocytes from both humans and mice.[10,14] However, the role of *CKAP5* in the pathogenesis of POI in vivo remains unclear.

In this study, we identified an association between *CKAP5* expression insufficiency and reduced ovarian function in patients with diminished ovarian reserve (DOR), validated by gene burden analysis in a cohort of patients with POI and controls, suggesting *CKAP5* as a gene involved in the regulation of ovarian ageing. A comparison between *Ckap5* heterozygous and wild-type mice revealed that the former exhibited a phenotype characteristic of POI, with a reduced ovarian primordial follicle pool and accelerated follicular atresia. Single-cell RNA sequencing (scRNA-seq) and single-oocyte sequencing analysis suggested that ovarian ageing in *Ckap5* heterozygous mice may be due to impaired DNA damage repair and autophagy, leading to increased follicular apoptosis, reduced oocyte quantity and compromised oocyte quality. Co-immunoprecipitation coupled with mass spectrometry and in vitro cell experiments identified ATM and ATG7 as key targets regulated by CKAP5 in the DNA damage repair and autophagy pathways. We also identified a loss-of-function variant in the *CKAP5* gene in clinical pedigrees with POI.

Methods

Clinical samples

A total of five DOR patients and five control patients who underwent in vitro fertilization (IVF)-embryo transfer or intracytoplasmic sperm injection at the Reproductive Medicine Centre of the Second Xiangya Hospital of Central South University were enrolled in this study from November 2021 to November 2022. The inclusion criteria for DOR patients included age <40 years, body mass index (BMI) < 25 kg/m^2, Anti-Müllerian hormone (AMH) < 1.1 ng/mL, and bilateral antral follicle count (AFC) < 6, according to the committee opinion from Practice Committee of the American Society for Reproductive Medicine.[15] Patients with female fallopian tube or male-related factors were selected as the control group. Patients with chromosomal abnormalities, endocrine disorders, endometriosis, recurrent miscarriage, a history of ovarian surgery, pelvic radiotherapy or chemotherapy, and autoimmune diseases were excluded. Ovarian stimulation was performed prior to the collection of oocytes by FSH (Lishenbao, Livzon) and human chorionic gonadotropin (hCG, Livzon). After consent was obtained from all enrolled patients, follicular fluid was collected for the isolation of granulosa cells (GCs). The follicular fluid was centrifuged at 1500 rpm for 10 min and then transferred into lymphocyte separation medium (P8800, Solarbio) to separate human GCs according to the manufacturer's instructions. The human GCs were stored at –80 °C for further research.

Members of two Han Chinese families with POI participated in this study. Peripheral blood samples were collected after the participants provided their written informed consent to participate in this study and agreed to the publication of this case report.

Analysis of RNA sequencing (RNA-seq) data of human GCs from patients

Differentially expressed genes (DEGs) were identified using the DESeq R package. P value < 0.01 and |Fold Change| > 1.5 were set as the threshold for significantly differential expression. Principal component analysis (PCA) of DEGs was performed to explore gene expression patterns. Gene ontology (GO) enrichment and REACTOME pathway enrichment analysis of DEGs were performed using the clusterProfiler R package. All genes were selected for weighted gene co-expression network analysis using the weighted gene co-expression network analysis (WGCNA) R package. The power of $\beta = 8$ was chosen as the soft-thresholding parameter to ensure an unsigned scale-free network. In WGCNA analysis, the correlation between modules and clinical phenotypes, as well as gene significance and module membership, was assessed using Pearson correlation analysis, with a significance threshold set at P value < 0.05. For genes in the turquoise module, when geneModuleMembership > 0.90 & geneTraitSignificance > 0.80 & GSPvalue < 0.05 & datKME > 0.90 & kIM > 1000, they were identified as hub genes in the module.

Gene burden analysis

In total, 93 patients with POI were recruited from the Xiangya Second Hospital of Central South University, the Changsha Reproductive Medicine Hospital and the Changsha Jiangwan Maternity Hospital. Whole-exome sequencing data were collected previously.[16] In total, 465 healthy women aged 45–65 years in the menopause stage (who had no amenorrhoea and regular menstrual cycles before age 40) were recruited from the Third Affiliated Hospital of Southern Medical University. Whole-genome sequencing data were collected previously.[17]

Gene-burden analysis of five candidate genes was performed. The following filtering thresholds were applied: read depth >30; variant allele frequency >0.3; minor allele frequency <1% in GnomAD, ExAC, and 1000 Genomes Phase 3. Genes were weighted using the SKAT-O method, and associations between genetic variants and POI were evaluated.

Whole-exome sequencing (WES) and variants filtration

Prior to WES, karyotype analysis was performed to exclude chromosomal abnormalities. The data were filtered for rare variants according to the following criteria: (1) autosomal or X-linked dominant and recessive inheritance; (2) variants that potentially affect protein sequence (nonsense, missense, splicing-site variants, or coding indels); (3) minor allele frequencies <0.01 in public databases, including 1000 Genomes, ExAC, and gnomAD. After filtering for known POI-related genes, no pathogenic variants in established POI genes were identified. The heterozygous *CKAP5* variant was then confirmed through family segregation analysis. Sanger sequencing was performed to validate the variant, with primers listed in Supplementary Table S8.

Co-immunoprecipitation (Co-IP) and mass spectrometry detection

The cells were washed with PBS buffer three times and discarded. Subsequently, IP lysis buffer (PC105, Epizyme Biotech) was added for digestion, followed by centrifugation at 12,000*g* at 4 °C for 15 min. The supernatant was mixed with anti-CKAP5 antibody at 4 °C overnight. Subsequently, magnetic beads were added and mixed uniformly overnight on a shaker at 4 °C. The eluted products were separated by gel electrophoresis and transferred to an activated PVDF membrane for detection. Finally, mass spectrometry analysis of the products was performed by BGI Genomics.

Animals

Ckap5-knockout mice were generated using CRISPR/Cas9 technology on a C57BL/6J genomic background. The sgRNA sequence and primers used for genotyping are provided in Supplementary Table S4. *Ckap5* systemic knockout mice with disrupted ORF were generated. Mice were maintained in a well-controlled, specific pathogen-free facility with 40–60% humidity, a constant temperature of 25 °C, and a 12-h light/dark cycle. The animal experiments were approved by the Animal Ethics Committee of Hunan University of Traditional Chinese Medicine. The care and experimental procedures for the mice were in accordance with the Institutional Guidelines of the Animal Care and Use Committee (ACUC) and were approved by the ACUC of the Hunan University of Traditional Chinese Medicine. Female mice ($Ckap5^{+/+}$ and $Ckap5^{+/-}$) were randomly selected and compared at each time point.

Mouse serum hormone assay

Blood samples were collected from $Ckap5^{+/+}$ and $Ckap5^{+/-}$ female mice from the age of 3, 6 and 9 months. Based on the anticipated effect sizes, the analysis indicated that a sample size of 4 mice per group would provide adequate power (0.8) to detect the expected differences at a significance level of 0.05. Serum was prepared and stored at –80 °C until use. Levels of serum FSH, luteinizing hormone (LH) and Oestradiol (E_2) were detected with mouse ELISA kit (JL10239, JL10432 and JL11232, JonlnBio), according to the manufacturers' instructions.

Fertility test
Female mice (n = 3 per group) were continuously mated with fertile male mice from 8 weeks to 36 weeks of age (female: male = 1:1). The numbers of pups and litters were recorded.

Histology of ovarian tissue
Ovarian tissues (n = 3 per group) were collected and fixed in 4% paraformaldehyde, embedded in paraffin, and serially sectioned at a thickness of 4 μm. Each sample was stained with haematoxylin and eosin (H&E). Ovarian follicles at different stages were counted according to the well-established standards.[18]

Picrosirius red (PSR) staining
The PSR Stain Kit (G1472, Solarbio) was used according to the manufacturer's protocol. Briefly, ovarian sections underwent deparaffinization with xylene and an ethanol gradient, followed by washes with water. Subsequently, sections were treated with PSR staining solution for 15 min at room temperature.

Analysis of scRNA-seq data of ovaries
Gene expression matrices were merged to create a single Seurat object and filtered based on the number of features (>400) and the percentage of mitochondrial transcripts (<25%). Genes expressed in fewer than three cells were excluded from the analysis. Variable genes were identified using the 'FindVariableFeatures' function, and 2000 variable genes were selected for subsequent analysis. The first 40 principal components were utilized for PCA. All data were combined using the Harmony R package to eliminate batch effects. Clustering was performed using the 'FindClusters' function, which operates on a k-nearest neighbour graph model with a resolution of 0.2, and results were displayed in uniform manifold approximation and projection (UMAP)/t-distributed stochastic neighbour embedding plots. The cell type of each cluster was identified using known marker genes with the 'FeaturePlot' function generated by the Seurat package. Subsequently, differential gene expression analysis was conducted using the 'FindMarkers' function of Seurat in the *Ckap5*$^{+/+}$ and *Ckap5*$^{+/-}$ groups. DEGs were defined as those genes with adjusted *P* values < 0.05 and |Fold Change| > 2. GO and GSEA enrichment analyses were performed in each cell type. To assess cell-to-cell interactions among different ovarian cell types in *Ckap5*$^{+/+}$ and *Ckap5*$^{+/-}$ mouse ovaries, we utilized the CellChat R package, which is based on the expression of known ligand–receptor pairs.

Oocyte collection
Mice were superovulated (n = 3 per group) via an intraperitoneal injection of 10 IU of pregnant mare serum gonadotropin. After 44–48 h, oocytes were collected from antral follicles by puncturing with a 26.5-gauge needle in M2 medium (M7167, Sigma–Aldrich).

Oocyte RNA sequencing and analysis
Smart-seq2 analysis were constructed using oocyte RNA from the *Ckap5*$^{+/+}$ and *Ckap5*$^{+/-}$ group (n = 3 per group), and the libraries were sequenced on the DNBSEQ sequencing platform (BGI Genomics). Differential gene expression analysis between the two groups was performed using DESeq2 R package. Genes with an adjusted *P* value below 0.05 and |Fold Change| > 2 were considered to be differentially expressed genes. The data were then subjected to GO and GSEA enrichment analysis.

Reactive oxygen species (ROS) level monitoring
To measure the ROS content, GV oocytes were incubated in M2 medium with DCFH-DA reagent prepared according to the manufacturer's instructions (AKCE002-1, Boxbio) at 37 °C for 20 min in a 5% CO_2 incubator. After washing three times with M2 medium, images of the oocytes were captured under the microscope.

Cell culture
Human embryonic kidney (HEK) 293T cells (RRID: CVCL_0063) were cultured in Dulbecco's Modified Eagle Medium (L110KJ, Basal Media) with 10% foetal bovine serum (11011-8611, Every Green) at 37 °C in a humidified 5% CO_2 incubator. Starvation-induced autophagy was induced by culturing the cells in Earle's Balanced Salt Solution (EBSS) (C0213, Beyotime) for 6 h. Chloroquine (CQ) (50-63-5, Sigma–Aldrich) was used at 20 μM to block autophagic degradation.

Gene silencing
Specific small interfering RNAs (siRNAs) targeting human *CKAP5* were generated by RiboBio. SiRNA was administered to cells using riboFECT CP Reagent from the kit (SIGS0003355-4, Ribobio) at 100 nM. The transfected cells were incubated at 37 °C for 72 h and then harvested for subsequent assays.

Plasmid generation and transfection
The wildtype his-*CKAP5* plasmid was generated by fusing the *CKAP5* cDNA fragment into pcDNA3.1 plasmid with N-terminal his tags. The mutant his-CKAP5 plasmid was generated according to the splicing result of minigene assay. Plasmids were transfected into HEK293T cells using the PolyJet In Vitro DNA Transfection Reagent (SL100688, SignaGen) according to the manufacturer's instructions.

Minigene assay
The wild-type and mutant Exon 5-intron 5-Exon 6 of human *CKAP5* complementary DNA (cDNA) fragments were cloned into a modified pcDNA3.1 plasmid. Subsequently, both plasmids were transfected into HEK293T cells using Lipofectamine 2000 (11668027, ThermoFisher), respectively. After culturing for 24 h, total RNA was extracted, and reverse transcribed into

cDNA. PCR products were purified by agarose gel electrophoresis and subjected to Sanger sequencing.

Western blot (WB) analysis

Tissues and cells were extracted using RIPA buffer (WB3100, NCM), supplemented with phenylmethanesulfonyl fluoride (1:100, AWH0642a, Abiowell) and Phosphatase Inhibitor Cocktail (1:100, AWB0159a, Abiowell). The proteins were separated by SDS-PAGE and subsequently transferred to a PVDF membrane. The membrane was blocked with a non-protein blocking solution (AR0041, Boster) and incubated with primary antibodies overnight at 4 °C. After three washes, the membranes were incubated with HRP-conjugated secondary antibodies at room temperature and then washed three times with TBST. Images were captured using a chemiluminescence detection system. The antibodies used are listed in the Supplementary materials. All primary antibodies were validated with bands of the expected molecular weights and correct localization of the target proteins.

Immunofluorescence (IF) and immunohistochemistry (IHC) assays

Isolated oocytes were fixed with 4% paraformaldehyde for 1 h at room temperature and permeabilized with 0.01% Triton X-100 for 15 min. After washing with PBS three times, oocytes were blocked with 5% BSA for 1 h and then incubated with the primary antibody overnight at 4 °C. Oocytes were washed again, incubated with secondary antibodies and stained with DAPI (P0131, Beyotime). The fluorescence of oocytes was observed using a microscope.

The sections of mouse ovaries were deparaffinized in xylene, dehydrated in a decreasing alcohol gradient, and underwent antigen retrieval by heating in sodium citrate buffer. Following blocking with 5% BSA, the sections were incubated with the primary antibody overnight at 4 °C. Subsequently, the sections were incubated with an HRP-conjugated secondary antibody and developed into colour using DAB (ZLI-9018, ZSGB-BIO). Nuclear staining was achieved with Haematoxylin before capturing images. In immunofluorescence experiments, sections were incubated with fluorescence-conjugated secondary antibodies and counterstained with antifade mounting medium with DAPI before observation under a fluorescence microscope.

All primary antibodies were validated with bands of the expected molecular weights and correct localization of the target proteins. The specificity of secondary antibody binding was confirmed by the absence of signal in negative controls incubated without primary antibodies.

TUNEL assay

Paraffin-embedded ovarian tissue sections were deparaffinized. The TUNEL assay was conducted according to the manufacturer's protocol (E-CK-A331, Elabscience).

Ethics statement

The animal study was reviewed and approved by the ACUC of Hunan University of Traditional Chinese Medicine (SLBH-202205160008). All methods were conducted in accordance with the ARRIVE guidelines.

For the study involving patients, this research was approved by the Ethics Committee of the School of Basic Medical Sciences, Central South University (2022-KT110), and written informed consent was obtained from all participants.

Statistics

For two-sample comparisons, normality and homogeneity of variance were assessed using the Shapiro–Wilk test and the F-test, respectively. When both normality and homogeneity of variance were satisfied, an independent t-test (Student's t-test) was performed. If normality was met but variances were unequal, Welch's t-test was applied. For data that did not meet the normality assumption, the Mann–Whitney U test was used. For comparisons involving three groups, a One-Way Analysis of Variance (ANOVA) was conducted to determine overall group differences. Post hoc analysis was performed using Tukey's multiple comparison test to assess pairwise differences between groups. The data are presented as the mean ± SEM. All P values, sample sizes ("n"), and statistical tests were specified in the figure legends. A P value of <0.05 was considered statistically significant. $^{*}P < 0.05$, $^{**}P < 0.01$, $^{***}P < 0.001$, $^{****}P < 0.0001$ and "ns" represents not significant. For the majority of experiments, we performed three biological replicates per group. This sample size was determined based on previous studies in the literature that assessed similar experimental conditions and outcomes, and was deemed sufficient for detecting meaningful differences given the nature of the experiments.[19] All treatments and outcome assessments were performed blindly, with experimenters unaware of group allocations to minimize bias.

Role of funders

The funders played no role in the study design, data collection, data analyses, interpretation, or writing of the manuscript.

Results

Differential gene expression in GCs from DOR and control patients

Following the established inclusion criteria, human GC samples were obtained from patients with DOR and controls (Fig. 1a). Compared to controls, patients with DOR exhibited significantly reduced levels of AMH and bilateral AFC (Supplementary Table S1). Total RNA was extracted from the human GCs for RNA library construction and sequencing (Supplementary Fig. S1a). PCA was performed, and PC1 revealed distinct

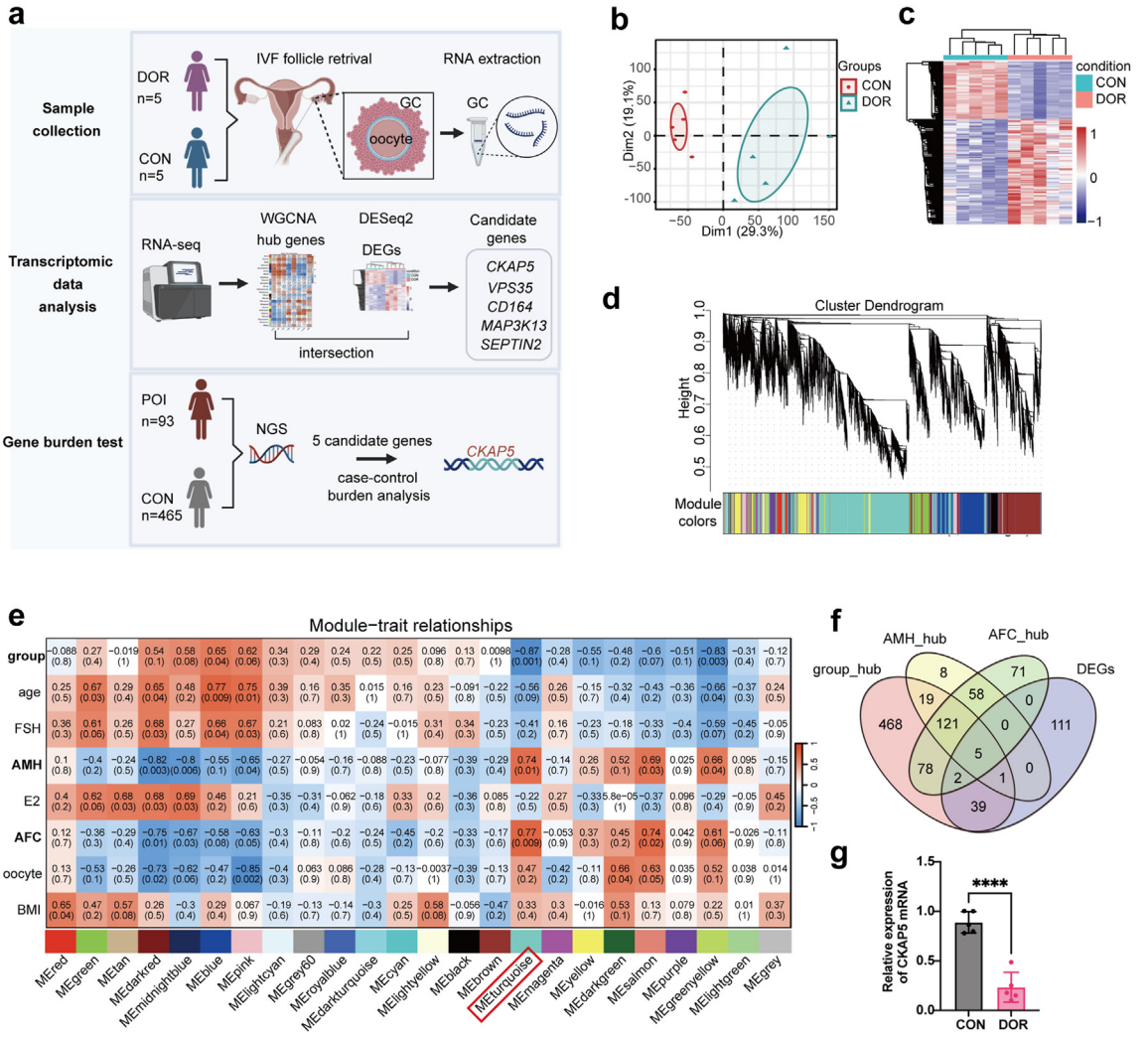

Fig. 1: Identification of *CKAP5* as a hub gene for ovarian ageing. a. The flowchart of identification of *CKAP5* as a hub gene for ovarian ageing. b. PCA analysis of RNA transcriptomes in the DOR vs. CON cohort (n = 5 for each group). c. Heatmap of DEGs. Red indicates upregulated genes and blue indicates downregulated genes in the DOR group (n = 5 for each group). d. The cluster dendrogram and hierarchical clustering heatmap of module eigengenes. e. The heatmap of correlation between genes in different modules and the clinical traits through WGCNA analysis. f. Venn diagrams of candidate genes obtained through intersecting the hub genes in turquoise module and DEGs. g. The verification of *CKAP5* by qRT−PCR in the DOR vs. CON cohort (n = 5, Student's t-test, ****$P < 0.0001$). DOR, diminished ovarian reserve; CON, control; CKAP5, Cytoskeleton Associated Protein 5; WGCNA, weighted gene co-expression network analysis; DEGs, differentially expressed genes; PCA, principal component analysis; oocyte, the number of follicles over 14 mm on HCG Day.

expression patterns between the DOR and control groups (Fig. 1b). Using expression profiling, we identified 158 DEGs. Compared to the control group, 102 genes were upregulated, and 56 genes were downregulated in patients with DOR, as shown in the heatmap (Fig. 1c and Supplementary Fig. S1b). GO and REACTOME enrichment analyses of the DEGs indicated that DOR was associated with intracellular macromolecule transport and maintenance of cellular structure (Supplementary Fig. S1c and d). Gene Set Enrichment Analysis (GSEA) indicated that the gene set related to DNA damage repair was downregulated (Supplementary Fig. S1e).

To identify the genes implicated in diminished ovarian function and their relationship with the DOR phenotype, WGCNA was performed using all the genes and clinical traits mentioned above (Supplementary Table S1). We identified 22 distinct gene modules within the cluster dendrogram and hierarchical clustering heatmap of module eigengenes (Fig. 1d and Supplementary Fig. S1f–g). Module-trait relationships revealed correlations between genes in various modules

and clinical traits (Fig. 1e). Red modules exhibited positive correlations, whereas blue modules displayed negative correlations. The turquoise module exhibited the highest positive correlation with AMH (r = 0.74, $P = 0.01$) and AFC (r = 0.77, $P = 0.009$), and the strongest negative correlation with the group (r = –0.87, $P = 0.001$). For these three traits, we found that the correlation between module membership and gene significance in the turquoise module was 0.66, 0.69, and 0.84, respectively, demonstrating a strong association between the genes in the turquoise module and the clinical features of DOR (Supplementary Fig. S1h and i). Using this method, we established thresholds for genes within the turquoise module to identify hub gene sets associated with three traits, AFC_hub, AMH_hub, and Group_hub, which contained 335, 212, and 733 hub genes, respectively. Intersecting these hub gene sets with 158 DEGs, five candidate genes were identified: *CKAP5*, *MAP3K13*, *CD164*, *VPS35*, and *SEPTIN2* (Fig. 1f).

Identification of *CKAP5* as a hub gene associated with ovarian ageing

For the five candidate genes, we conducted gene burden analysis using next-generation sequencing data from 93 patients with POI and 465 healthy female controls in the Chinese population (Supplementary Tables S2–S3). The results revealed that *CKAP5* exhibited the highest significance ($P = 1.86 \times 10^{-3}$) and variant frequency in the POI group (5.38%) in the Chinese population. In addition, reverse transcription polymerase chain reaction (RT-PCR) confirmed that *CKAP5* mRNA levels were significantly lower in the DOR group than in the control group (Fig. 1g). Previous in vitro studies have demonstrated that *CKAP5* plays a critical role in oocyte meiosis, embryo development, and cell proliferation. Based on these findings, we selected *CKAP5* for further investigation in animal experiments.

Characterization of CKAP5 expression in ovarian tissue

Normal follicle development requires both the oocyte and surrounding GCs to be in optimal conditions. CKAP5 was predominantly expressed in oocytes and GCs across various follicular stages in mouse ovaries (Fig. 2a), especially during the primordial and primary follicle stages. As follicles develop further, starting from the secondary follicle stage, CKAP5 is highly expressed in both oocytes and GCs.

CKAP5 is expressed in germinal vesicle (GV) oocytes and colocalizes with microtubule asters (Fig. 2b). As oocytes progress from germinal vesicle breakdown (GVBD) onwards, CKAP5 aggregates around chromosomes within the spindle region. At both the metaphase I (MI) and metaphase II (MII) stages, CKAP5 was concentrated around aligned chromosomes, indicating its critical role in oocyte maturation (Fig. 2b).

To investigate the role of *CKAP5* in female fertility in vivo, a knockout mouse model of *Ckap5* was generated (Fig. 2c, Supplementary Table S4). Homozygous deletion of *Ckap5* impairs early embryonic development[14] and results in embryonic lethality.[20] Therefore, only heterozygous *Ckap5*-deficient mice were available for the subsequent experiments (Supplementary Table S5). Genotyping of the $Ckap5^{+/-}$ mice was confirmed by PCR and Sanger sequencing (Fig. 2d and Supplementary Fig. S2a and b) with protein loss verified by WB (Fig. 2e and f) and IHC staining (Fig. 2g) of ovaries from 1-month-old mice.

Ckap5 knockout results in subfertility due to POI in mouse

While $Ckap5^{+/-}$ mice were viable (Supplementary Fig. S2c and d), their ovarian volume was significantly reduced compared to $Ckap5^{+/+}$ mice (Fig. 2h and i). Total pup numbers for $Ckap5^{+/-}$ females deviated markedly from those of $Ckap5^{+/+}$ females, indicating decreased fertility (Fig. 2j). Pregnant mare serum gonadotropin was used to induce superovulation in 4- and 12-week-old mice by collecting the oocytes. Compared to wild-type mice, the ovarian response in $Ckap5^{+/-}$ mice was significantly reduced, with a decrease in the number of retrieved oocytes by 59.32% and 69.86%, respectively (Fig. 2k). Collectively, $Ckap5^{+/-}$ mice exhibited an earlier decline in fertility compared to $Ckap5^{+/+}$ mice.

We conducted additional analyses of sex hormone and ovarian tissues from mice to elucidate the POI phenotype in $Ckap5^{+/-}$ mice. Elevated levels of FSH and LH, along with decreased levels of E_2, were detected in the serum of $Ckap5^{+/-}$ mice at 3, 6, and 9 months of age. Starting at 3 months, FSH levels in $Ckap5^{+/-}$ mice were significantly elevated, consistent with the hormonal abnormalities associated with POI observed in humans (Fig. 2l). With advancing age, E_2 levels declined significantly at 6 and 9 months of age, accompanied by elevated LH levels (Fig. 2l). Histological analysis of ovarian tissue sections stained with H&E revealed a reduction in the number of primordial and primary follicles starting from 1 month after birth in $Ckap5^{+/-}$ mice (Fig. 2m). In adulthood, there was a significant decrease in secondary and antral follicles in $Ckap5^{+/-}$ mice compared to $Ckap5^{+/+}$ mice, accompanied by increased follicle atresia (Fig. 2m). These findings suggest that *Ckap5* haploinsufficiency leads to oocyte depletion and impaired fertility, indicating a phenotype consistent with POI.

ScRNA-seq reveals impaired DNA damage repair, autophagy, and increased apoptosis in $Ckap5^{+/-}$ ovaries

To analyse the transcriptomic variation in ovarian cells, we performed scRNA-seq on the ovaries of three 3-month-old $Ckap5^{+/-}$ mice (Fig. 3a). Previously reported

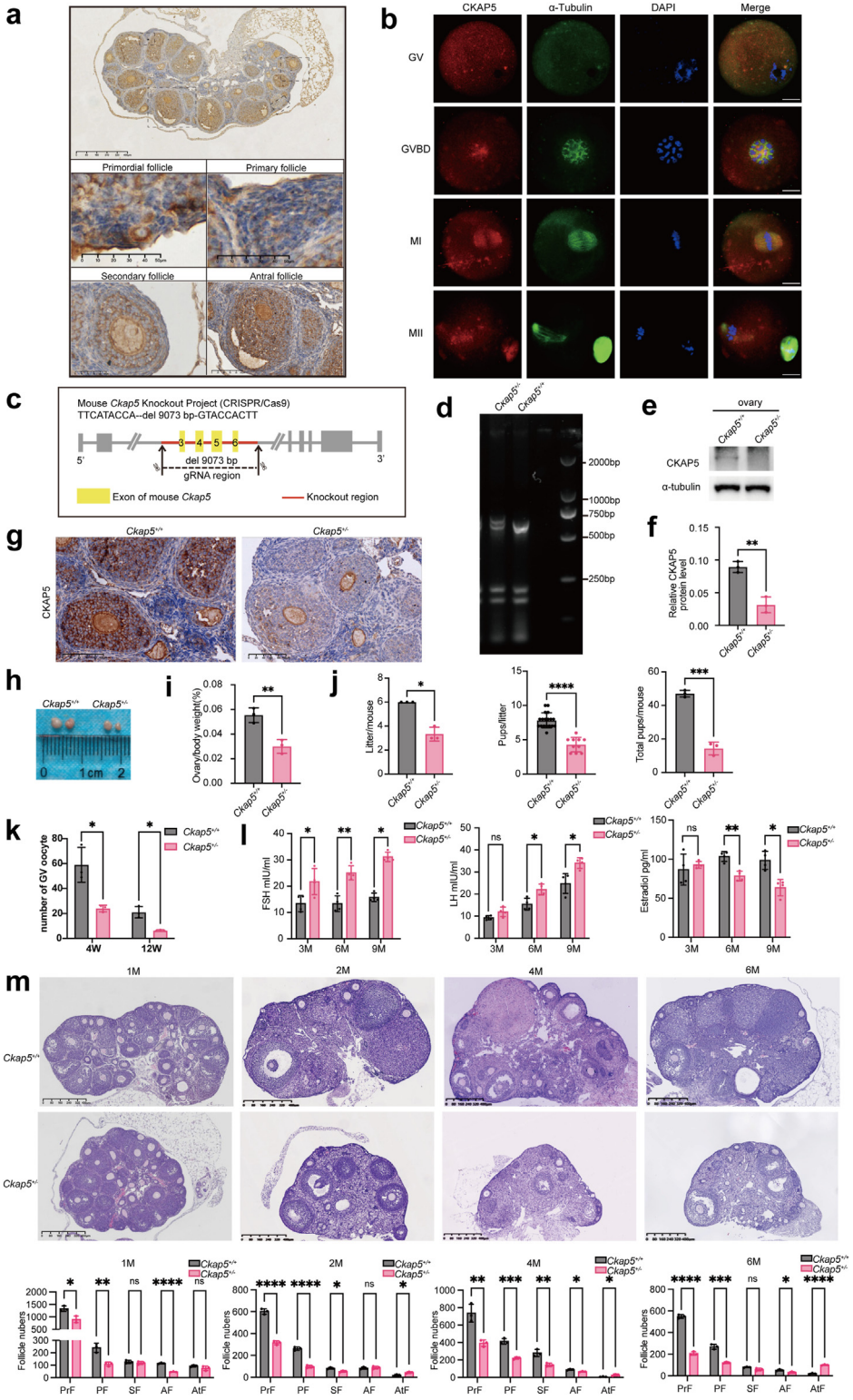

Fig. 2: *Ckap5* knockout results in subfertility due to POI in mouse. a. Immunohistochemistry of CKAP5 in ovarian sections from 1-month-old wildtype mice. Scale bars denote 50 μm, 100 μm and 400 μm. b. Immunofluorescence analysis for CKAP5 and α-tubulin colocalization in the oocyte maturation from wildtype adult mice. Scale bars denote 20 μm. c. Schematic diagram of *Ckap5* knockout. CRISPR/Cas9 technology was

scRNA-seq data from 3-month-old normal ovaries were reanalysed as a control using the same methodology.[21] After rigorous cell filtration, a total of 19,717 cells were retained for further analysis (Supplementary Fig. S3a and b). Batch effects were corrected using the Harmony R package, and global ovarian cell populations were visualized using UMAP (Fig. 3b and Supplementary Fig. S3c). This analysis identified 10 distinct cell types based on specific marker expression[21]: oocytes, GCs, luteal cells, theca cells, stromal cells, macrophages, T cells, B cells, endothelial cells and epithelial cells (Supplementary Fig. S3d). *Ckap5* was predominantly expressed in non-immune cells (Supplementary Fig. S3e). Notably, the clustering results showed that *Ckap5*$^{+/-}$ ovarian cells were well-distributed compared to normal controls (Fig. 3c and Supplementary Fig. S3c). In addition, CKAP5 deficiency altered ovarian cellularity compared to controls (Fig. 3c, Supplementary Table S6). The percentage of oocytes and GCs was significantly lower in *Ckap5*$^{+/-}$ ovaries, which can be attributed to the decline in the number of follicles observed. The most notable change in ovarian cellularity associated with CKAP5 deficiency was a two-fold increase in stromal, endothelial, and epithelial cells. The percentage of immune cells in the ovaries of *Ckap5*$^{+/-}$ mice was slightly decreased. These results indicate a decline in follicles and an increase in stromal tissue accumulation in *Ckap5*$^{+/-}$ mice.

Next, GO enrichment analysis was performed for each cell type. Autophagy, DNA damage repair, oocyte development, fertilization, pregnancy, and steroid hormone-mediated signalling pathways were downregulated in most cells, whereas apoptosis and the negative regulation of cell development pathways were upregulated (Fig. 3d and e). Owing to the low number of oocytes captured from *Ckap5*$^{+/-}$ mice, no statistically significant pathways were identified in the GO enrichment analysis (Supplementary Table S6). Therefore, we conducted GSEA on oocytes. Similarly, "phagophore assembly site membrane" and "DNA damage sensor activity" gene sets were downregulated in the oocytes of *Ckap5*$^{+/-}$ mice, accompanied by an upregulation of "cell killing" gene sets (Fig. 3f and Supplementary Fig. S3f). This enrichment analysis shows that decreased autophagy, DNA damage repair, and increased apoptosis signalling in ovarian cells may account for the POI phenotype of the *Ckap5*$^{+/-}$ mice.

Aberrant cell-to-cell communication patterns in the ovary following CKAP5 deletion

Altered intercellular communication is an integrated hallmark of ageing.[22] CellChat analysis was conducted to evaluate signalling networks. Despite the decline in ovarian function in *Ckap5*$^{+/-}$ mice, intercellular communication was not completely disrupted (Supplementary Fig. S4a and b). A significant reduction in cell signal transduction was observed between oocytes and other cell types, while interactions between stromal cells and other cell types, particularly granulosa, luteal, and theca cells associated with follicles, increased (Supplementary Fig. S4a). All communication probabilities in the information network were summarized to compare the difference in overall information flow between *Ckap5*$^{+/-}$ and *Ckap5*$^{+/+}$ mice (Supplementary Fig. S4c). The results revealed that AMH signalling pathways were more abundant in *Ckap5*$^{+/+}$ mice, whereas COLLAGEN signalling pathways were more abundant in *Ckap5*$^{+/-}$ mice (Supplementary Fig. S4c–e).

Single-oocyte transcriptome analysis reveals CKAP5 deficiency impairs oocyte quality

To investigate the potential impact of CKAP5 deletion on oocyte quality, we conducted a single-cell transcriptome analysis of ovulated GV oocytes from 3-month-old mice using the SMART-seq2 method (Fig. 3a). RNA levels of *Ckap5* were significantly lower in *Ckap5*$^{+/-}$ oocytes than in *Ckap5*$^{+/+}$ oocytes (Supplementary Fig. S5a and b). PCA revealed distinct expression patterns between *Ckap5*$^{+/-}$ and *Ckap5*$^{+/+}$ oocytes, with PC1 showing clear separation (Fig. 3g). Heatmap analysis indicated that DEGs were primarily downregulated (Fig. 3h and Supplementary Fig. S5c) and enriched in pathways related to autophagy, reproductive processes, oocyte development, and oxidative

used to generate *Ckap5*$^{+/-}$ mice by deleting exon 3 to exon 6. d. Genotype of *Ckap5*$^{+/+}$ and *Ckap5*$^{+/-}$ mice. Heterozygotes: two bands with 714 bp and 643 bp. Wild-type allele: one band with 643 bp. e. Western blot analysis of CKAP5 in ovary from *Ckap5*$^{+/+}$ and *Ckap5*$^{+/-}$ mice. f. Relative protein levels of CKAP5 in ovary from *Ckap5*$^{+/+}$ and *Ckap5*$^{+/-}$ mice (n = 3, Student's t-test, $^{**}P < 0.01$). Relative amounts of proteins were calculated after normalization to the α-tubulin protein level. g. Immunohistochemistry analysis of CKAP5 expression in the ovary from *Ckap5*$^{+/+}$ and *Ckap5*$^{+/-}$ mice. Scale bars denote 100 μm. h. The ovarian development of *Ckap5*$^{+/+}$ and *Ckap5*$^{+/-}$ female adult mice. i. The ovary/body weight of *Ckap5*$^{+/+}$ and *Ckap5*$^{+/-}$ female adult mice (n = 3, Student's t-test, $^{**}P < 0.01$). j. The numbers of litters per mouse, the number of pups per litter and the numbers of total pups per mouse were recorded for each group in the fertility test (n = 3, Welch's t-test, litter/mouse: $^{*}P < 0.05$; Mann–Whitney test, pups/litter: $^{****}P < 0.0001$; Student's t-test, total pups/mouse: $^{***}P < 0.001$). k. GV oocytes obtained from *Ckap5*$^{+/-}$ and *Ckap5*$^{+/+}$ mice at 4 and 12 weeks old (n = 3, Student's t-test, 4w: $^{*}P < 0.05$; Welch's t-test, 12w: $^{*}P < 0.05$). l. Serum FSH, LH and E_2 levels of 3-month-old, 6-month-old and 9-month-old *Ckap5*$^{+/+}$ and *Ckap5*$^{+/-}$ mice (n = 4, 3 and 6 months: Student's t-test; 9 months: Mann–Whitney test; $^{*}P < 0.05$, $^{**}P < 0.01$). m. HE staining and comparison of the numbers of follicles of mice at 1-month-old, 2-month-old, 4-month-old and 6-month-old (n = 3, Student's t-test, $^{*}P < 0.05$, $^{**}P < 0.01$, $^{***}P < 0.001$, $^{****}P < 0.0001$). Scale bars denote 400 μm. GV, germinal vesicle stages; GVBD, germinal vesicle breakdown stages; MI, metaphase I stages; MII, metaphase II stages; PrF, primordial follicle; PF, primary follicle; SF, secondary follicles; AF, antral follicle; AtF, atresia follicle; FSH, Follicle-stimulating hormone; E_2, Oestradiol; LH, Luteinizing hormone.

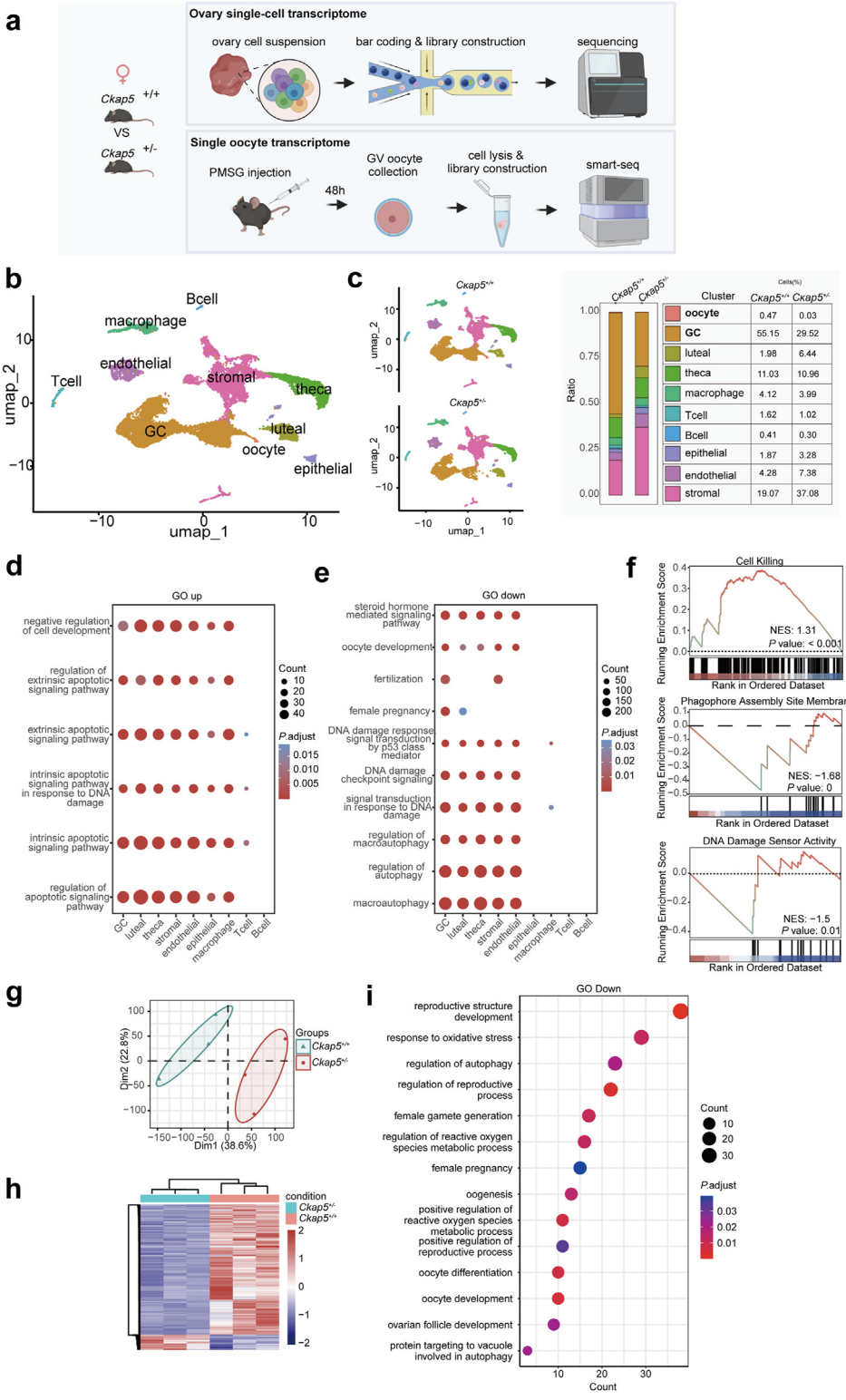

Fig. 3: ScRNA-seq analysis reveals the decreased autophagy and DNA damage repair along with increased apoptosis in ovaries of *Ckap5*$^{+/-}$ mice. a. The flowchart of ovary scRNA-seq and single-oocyte transcriptomic in *Ckap5*$^{+/-}$ and *Ckap5*$^{+/+}$ mice. b. UMAP plot of combined ovarian cells. Clustering analysis revealed 10 distinct ovarian cell populations. c. UMAP plot of ovarian cells by genotype. Numbers and percentages of cell type

stress (Fig. 4i). GSEA revealed downregulation in gene sets associated with cell growth, autophagy, and the P53 pathway, indicating a potential impairment in oocyte quality (Supplementary Fig. S5d).

CKAP5 binds to ATG7 and ATM as a downstream target

To elucidate how impaired autophagy and DNA damage repair are regulated in *Ckap5*$^{+/-}$ mice, we employed Co-IP coupled with mass spectrometry to identify proteins interacting with CKAP5 (Supplementary Fig. S6a and Table S7). Proteins interacting with CKAP5 are involved in autophagy, cell cycle and DNA damage repair, apoptosis, reproduction and meiosis, phosphatase and tensin homologue deleted on chromosome 10 (PTEN) regulation, and ROS detection, consistent with the enrichment analysis from previous scRNA-seq and single-oocyte transcriptome studies (Supplementary Fig. S6b). The list of interacting proteins was matched with the proteins encoded by known POI-associated pathogenic genes, revealing that CKAP5 interacts with ATM and ATG7 (Supplementary Fig. S6c). These two proteins, which may act downstream of CKAP5 to promote DNA damage repair and autophagy, were further validated by Co-IP using peripheral blood samples from healthy women and wildtype mouse ovaries (Supplementary Fig. S6d and e).

CKAP5 promotes repair of double-strand breaks (DSBs) to prevent aberrant DNA damage in the ovary

RNA interference was employed in HEK293T cells to downregulate CKAP5 expression and validate its regulatory mechanism. We examined the changes in the ATM-CHK2-P53 and ATM-SMC3/SMC1A pathways, which promote DNA damage repair (Fig. 4a and Supplementary Fig. S7a and b). CKAP5 downregulation reduced protein expression and phosphorylation in these two pathways. To confirm that CKAP5 deficiency impairs DNA damage repair, 100 nM etoposide was added to the cell culture medium to induce DSBs, and the cellular response was observed. Compared to the control group, CKAP5 deficiency resulted in decreased expression and phosphorylation of ATM-CHK2-P53 and ATM-SMC3/SMC1A, ultimately leading to the accumulation of the DSBs marker, γH2AX, and indicating impaired DNA repair (Fig. 4b and Supplementary Fig. S7c and d).

Moreover, the ATM-CHK2-P53 and ATM-SMC3/SMC1A pathways, along with their phosphorylation levels, were downregulated in *Ckap5*$^{+/-}$ mouse ovaries, leading to γ-H2AX accumulation, indicating unrepaired DNA damage (Fig. 4c and Supplementary Fig. S7e and f). These findings suggest that *Ckap5* haploinsufficiency may reduce the ovarian reserve by inhibiting DNA damage repair in mice. Similarly, ATM was downregulated in both oocytes and GCs of *Ckap5*$^{+/-}$ mice, and the expression patterns of its downstream molecules, CHK2-P53 and SMC3/SMC1A, followed suit (Fig. 4d and Supplementary Fig. S7g). However, unlike the global downregulation of p-CHK2 within the follicle, the decreased phosphorylation levels of P53, SMC3, and SMC1A were mainly confined to the oocytes (Supplementary Fig. S7g). These defects in the ATM-CHK2-P53 and ATM-SMC3/SMC1A pathways in *Ckap5*$^{+/-}$ mice led to unrepaired DSBs, as evidenced by strong γH2AX positivity in follicles (Fig. 4d). In addition, ATM colocalized with CKAP5 on the spindle during meiosis, which is essential for the meiotic process (Fig. 4e and Supplementary Fig. S7h). In *Ckap5*$^{+/-}$ mice, this co-localization was lost in oocytes, causing abnormal spindle formation.

CKAP5 promotes autophagosome formation to maintain ovarian autophagy flux

In addition to DNA damage repair, we examined changes in autophagy. CKAP5 downregulation reduced ATG7 and ATG5 levels, lowering the LC3II/I ratio, a marker of autophagosome formation (Fig. 4f and Supplementary Fig. S8a). Immunofluorescence revealed scattered autophagosomes in the cytoplasm of the control group, whereas the si-*CKAP5* group exhibited a significant reduction in dot-like structures (Fig. 4g and Supplementary Fig. S8b). P62, a substrate for autophagolysosome fusion, accumulated in CKAP5-deficient cells, indicating impaired autophagosome formation and disrupted autophagic flux (Fig. 4f and Supplementary Fig. S8a). Under physiological conditions, cellular autophagic activity is typically low. To further investigate autophagy, we used the autophagy inducer EBSS and/or the autophagic degradation inhibitor CQ in both cell groups (Fig. 4h–i and Supplementary Fig. S8c and d). Consistent with previous results, ATG5 and ATG7 levels decreased with CKAP5 downregulation, accompanied by a decrease in LC3II and P62 accumulation (Fig. 4h–i and Supplementary Fig. S8c and d). Unexpectedly, under EBSS and/or CQ treatment, ATG3 exhibited an expression trend similar to that of CKAP5, suggesting that ATG3 may also function as a downstream protein of CKAP5 to promote autophagy.

identity by genotype. d. GO enrichment analysis of genes of up-regulated DEGs in different cell types. e. GO enrichment analysis of genes of down-regulated DEGs in different cell types. f. GSEA enrichment analysis of the oocyte for the pathways related to autophagy, DNA damage repair, and cell killing. g. PCA analysis of oocyte RNA transcriptomes form *Ckap5*$^{+/-}$ and *Ckap5*$^{+/+}$ mice. h. Heatmap of DEGs. Red indicates upregulated genes and blue indicates downregulated genes in the *Ckap5*$^{+/-}$ group. i. GO enrichment analysis of down-regulated DEGs. GO, gene ontology, GSEA, Gene Set Enrichment Analysis; NES, normalized enrichment score; DEGs, differentially expressed genes.

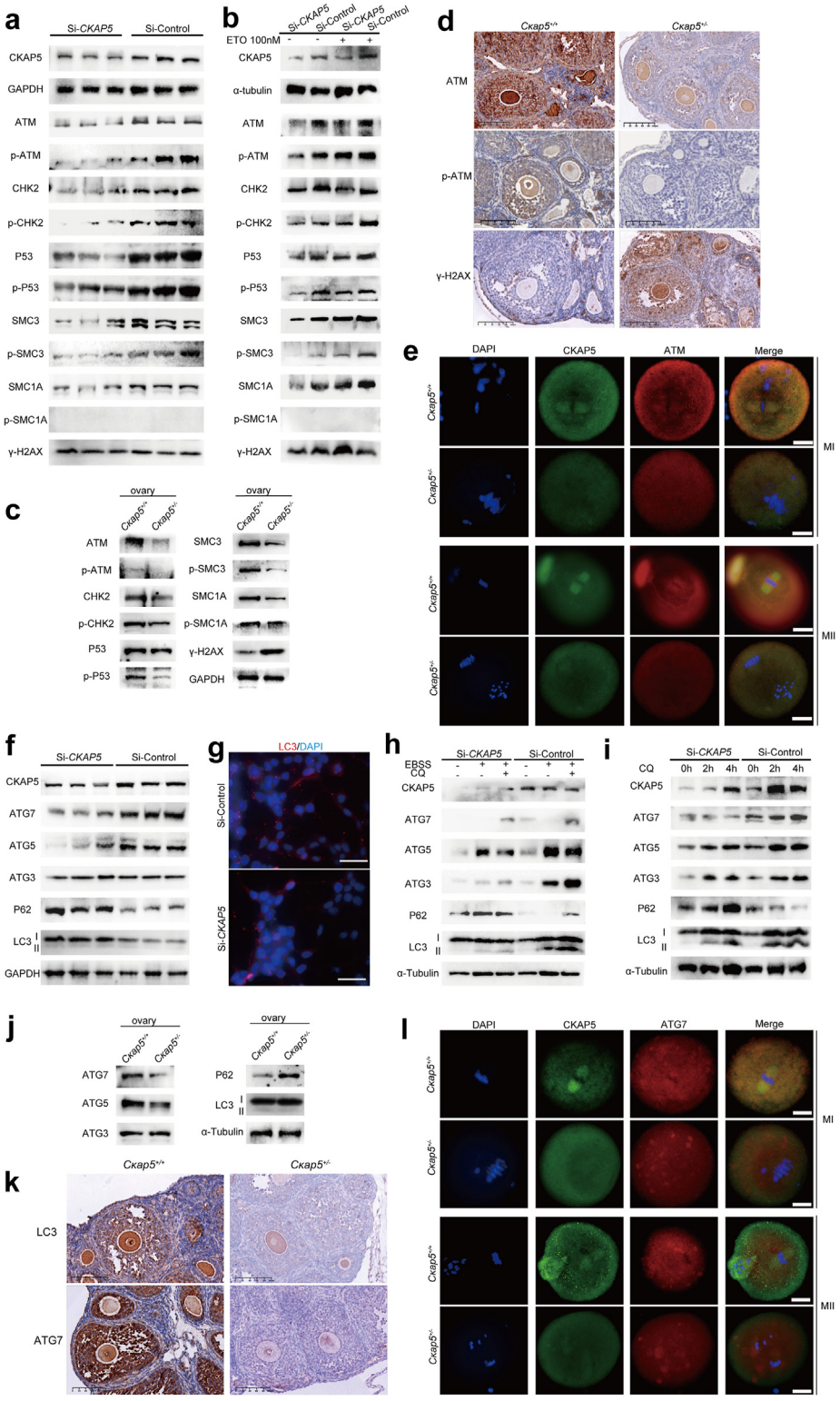

Fig. 4: CKAP5 promotes DSBs repair and autophagosome formation to prevent aberrant DNA damage and maintain ovarian autophagy flux. a. Protein levels of CKAP5, ATM, p-ATM, CHK2, p-CHK2, P53, p-P53, SMC3, p-SMC3, SMC1A, p-SMC1A and γ-H2AX in HEK293T cells transfected with si*CKAP5* and siControl as measured by Western blot. GAPDH was used as the loading control. b. Protein levels of CKAP5, ATM, p-ATM,

To determine whether the absence of CKAP5 leads to POI in mice through inhibition of the autophagy pathway, we analysed the differences in these autophagy-related proteins in the ovaries of *Ckap5*$^{+/+}$ and *Ckap5*$^{+/-}$ mice (Fig. 4j and Supplementary Fig. S8e). Consistent with the cellular experiments, the absence of CKAP5 resulted in decreased ATG7 levels, a lower LC3II/I ratio, and P62 accumulation in the ovaries (Fig. 4j and Supplementary Fig. S8e). In *Ckap5*$^{+/-}$ mice, ATG7 expression was significantly reduced in both oocytes and GCs, leading to decreased LC3 expression across the follicle, particularly in GCs (Fig. 4k). In addition, ATG7 colocalized with CKAP5 on the spindle during meiosis (Fig. 4l and Supplementary Fig. S8f); however, it was lost in *Ckap5*$^{+/-}$ oocytes, resulting in abnormal spindle formation.

These findings suggest that CKAP5 deficiency disrupts both autophagy and DNA damage repair, impairing overall follicle function and contributing to the onset of POI in mice.

Abnormal oocytes meiosis, accelerated ageing, and excessive apoptosis with collagen deposition in *Ckap5*$^{+/-}$ mouse ovaries

Previous studies have reported that deficiencies in autophagy and DNA damage repair lead to elevated apoptosis in the ovaries of mice.[23,24] We also measured the apoptosis levels in *Ckap5*$^{+/-}$ and *Ckap5*$^{+/+}$ mice. We found increased expression of the pro-apoptotic protein BAX, decreased expression of the anti-apoptotic protein BCL2, elevated levels of the activated effector protein CASPASE3, and increased TUNEL-positive staining in the *Ckap5*$^{+/-}$ ovaries, indicating elevated apoptosis levels (Supplementary Fig. S9a and b). The immunofluorescence results revealed that GCs exhibit more severe apoptosis, suggesting that GCs may play a more crucial role in follicular atresia (Supplementary Fig. S9c). The RNA-seq analysis and experimental results suggest that dysregulation of autophagy and DNA damage repair may contribute to the decline in ovarian reserve and increased apoptosis in *Ckap5*$^{+/-}$ mice. This indicates that the process of follicular atresia in *Ckap5*$^{+/-}$ mice is mediated by cell apoptosis.

Fibrosis accumulation in both follicular and non-follicular tissues is a canonical marker of ovarian ageing.[25] When examining collagen intercellular communication among cells, signalling in stromal cells from *Ckap5*$^{+/-}$ ovaries became stronger towards all cell types except T and B cells (Supplementary Fig. S4d). Notably, PSR staining for collagen revealed that CKAP5 deletion led to increased collagen accumulation in the follicular and stromal compartments of *Ckap5*$^{+/-}$ ovaries (Supplementary Fig. S9d). AMH levels reflect the number of follicles remaining in the ovary[26] and typically decline before elevated FSH concentrations. The AMH signalling pathway, which is indicative of ovarian function, was primarily downregulated in follicular cells (Supplementary Fig. S4e). IHC analysis confirmed lower AMH levels in the follicles of *Ckap5*$^{+/-}$ mice compared to *Ckap5*$^{+/+}$ mice (Supplementary Fig. S9e). These results suggest that CKAP5 deficiency disrupts the coordinated intercellular communication in *Ckap5*$^{+/-}$ mice, reducing overall ovarian function.

In oocytes from *Ckap5*$^{+/-}$ mice, spindle disorganization was observed (Supplementary Fig. S9f), accompanied by a decreased first polar body (PB1) extrusion rate of 40.67% (Supplementary Fig. S9g). Compared to *Ckap5*$^{+/+}$ mice, the rate of spindle abnormalities in *Ckap5*$^{+/-}$ oocytes increased by approximately 40.66% (Supplementary Fig. S9g). In addition, a significant accumulation of ROS was observed in *Ckap5*$^{+/-}$ GV oocytes, indicating oocyte ageing and potentially inducing DNA damage to the oocyte genome (Supplementary Fig. S9h). The *Ckap5*$^{+/-}$ mice exhibited a reduced oocyte count and abnormalities in oocyte quality, exacerbating the decline in female fertility.

CKAP5 variant causes mendelian inherited POI

In two Chinese Han families, probands exhibited menstrual irregularities following menarche and subsequently developed POI at 23 and 26 years of age (Fig. 5a). Ultrasonographic examination revealed

CHK2, p-CHK2, P53, p-P53, SMC3, p-SMC3, SMC1A, p-SMC1A and γ-H2AX in HEK293T cells transfected with si*CKAP5* and siControl or treated with ETO as measured by Western blot. α-Tubulin was used as the loading control. c. Protein levels of ATM, p-ATM, CHK2, p-CHK2, P53, p-P53, SMC3, p-SMC3, SMC1A, p-SMC1A and γ-H2AX in ovary from *Ckap5*$^{+/-}$ and *Ckap5*$^{+/+}$ mice as measured by Western blot. GAPDH was used as the loading control. d. Immunohistochemistry analysis for ATM, p-ATM and γ-H2AX in the ovary of *Ckap5*$^{+/+}$ and *Ckap5*$^{+/-}$ adult mice. Scale bars denote 100 μm. e. Immunofluorescence analysis for CKAP5 and ATM colocalization in the oocyte maturation from *Ckap5*$^{+/-}$ and *Ckap5*$^{+/+}$ mice. Scale bars denote 20 μm. f. Protein levels of CKAP5, ATG7, ATG5, ATG3, P62 and LC3 in HEK293T cells transfected with si*CKAP5* and siControl as measured by Western blot. GAPDH was used as the loading control. g. Immunofluorescence analysis for LC3 expression were decreased in HEK293T cells transfected with si*CKAP5*. Scale bars denote 200 μm. h. Protein levels of CKAP5, ATG7, ATG5, ATG3, P62 and LC3 in HEK293T cells transfected with siCKAP5 and siControl or pre-treated with EBSS and/or CQ as measured by Western blot. α-Tubulin was used as the loading control. i. Protein levels of CKAP5, ATG7, ATG5, ATG3, P62 and LC3 in HEK293T cells transfected with siCKAP5 and siControl or pre-treated with CQ for 0–4 h as measured by Western blot. α-Tubulin was used as the loading control. j. Protein levels of ATG7, ATG5, ATG3, LC3 and P62 in ovary from *Ckap5*$^{+/-}$ and *Ckap5*$^{+/+}$ mice as measured by Western blot. α-tubulin was used as the loading control. k. Immunohistochemistry analysis for ATG7 and LC3 in the ovary of *Ckap5*$^{+/+}$ and *Ckap5*$^{+/-}$ adult mice. Scale bars denote 100 μm. l. Immunofluorescence analysis for CKAP5 and ATG7 colocalization in the oocyte maturation from *Ckap5*$^{+/-}$ and *Ckap5*$^{+/+}$ mice. Scale bars denote 20 μm. DSBs, double strand breaks; ETO, etoposide; MI, metaphase I stages; MII, metaphase II stages; EBSS, Earle's Balanced Salt Solution; CQ, Chloroquine.

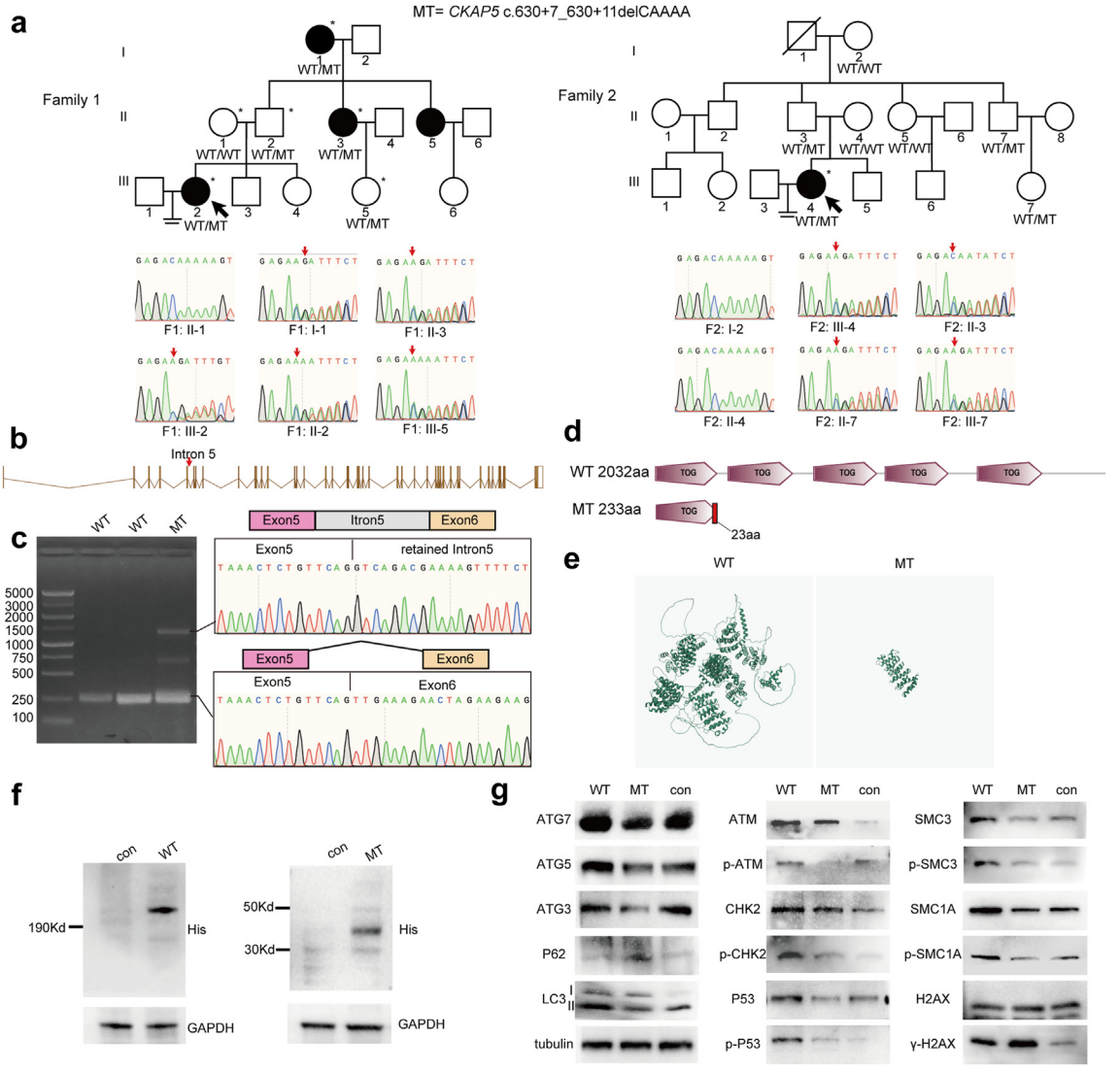

Fig. 5: CKAP5 variant causes clinical POI. a. The pedigrees of the families. Squares and circles denote male and female members, respectively. Solid symbols indicate the affected members, and open symbols denote unaffected members. Slashes represent deceased members, and the equal sign indicates infertility. Members indicated by arrows were probands. Members indicated by asterisk were selected for whole-exome sequencing. Sanger sequencing chromatograms of *CKAP5* are shown on the bottom side. The red arrows indicate the corresponding variant. b. Schematic map of the variant positions in *CKAP5* at the genomic level. c. Mini-gene assay of wild-type and mutated *CKAP5* plasmids transfected into HEK293T cells. Sanger sequencing of the band form mini-gene assay. d. Schematic map of the variant positions in CKAP5 at the protein level. e. Protein structure of wild-type and mutated CKAP5 predicted by Alphafold3. f. Wild-type and mutated *CKAP5* plasmids were transfected into HEK293T cells. After 72 h of transfection, whole-cell lysates were prepared and separated by SDS-PAGE. CKAP5 was detected by His antibody and GAPDH served as a loading control. Arrows indicate the targeted proteins. g. Protein levels of ATG7, ATG5, ATG3, LC3, P62, ATM, p-ATM, CHK2, p-CHK2, P53, p-P53, SMC3, p-SMC3, SMC1A, p-SMC1A and γ-H2AX in HEK293T cells transfected with wildtype and mutated *CKAP5* plasmids as measured by Western blot. α-Tubulin was used as the loading control. WT, wild type; MT, mutant type; con, control.

ovarian atrophy, with zero to one follicle in the probands. Serum FSH levels were elevated, whereas AMH levels were significantly decreased (Table 1), confirming POI diagnosis. Notably, the probands did not present with chromosomal abnormalities, a history of ovarian surgery, chemotherapy, radiotherapy, autoimmune diseases, or FMR1 premutations. To investigate the potential genetic causes, we conducted WES of three patients and three unaffected members in family 1 and one patient in family 2 (Fig. 5a and b). After filtering and sanger sequencing in members of two families, we identified a heterozygous *CKAP5* variant (NM_0001008938.4, c.630 + 7_630 + 11delCAAAA) that was consistent with the pattern of family co-segregation.

Predictions indicated that this variant, located in intron 5, might cause alternative splicing (Fig. 5b). Minigene experiments confirmed that the variant induced intron 5 retention by constructing a mini-gene plasmid that spanned from exons 5 to 6 and transfecting it into HEK293T cells (Fig. 5c and d). This in-frame insertion led to a premature termination codon (TGA) at the 70th nucleotide downstream of *CKAP5* exon 5.

Mutant plasmids were designed based on the complementary sequence of the spliced RNA. Both the wild-type and mutant plasmids were transfected into HEK293T cells and incubated for 72 h. Cellular experiments demonstrated that the mutant plasmids produced a truncated protein (Fig. 5d–f). Peripheral blood from the patient F2: III-4 was also analysed, and the results were consistent with the cellular experiments, showing a truncated protein (Supplementary Fig. S10a). Furthermore, compared to the wild-type plasmid transfection group, the group expressing the mutant protein exhibited reduced autophagy and DNA damage repair, consistent with the *CKAP5* knockdown results (Fig. 5g and Supplementary Fig. S10b–d). These findings suggest that CKAP5 truncation leads to loss of function, causing POI in patients.

Pedigree ID	Age	Age at menarche	Gestation and parturition	FSH (IU/L)	AMH (ng/mL)
F1: III-2	23	13	G0P0	30.85	0.66
F2: III-4	31	12	G0P0	26.05	0.01

FSH, Follicle-stimulating hormone; AMH, anti-Müllerian hormone.

Table 1: **Clinical data for the probands.**

Discussion

With the widespread application of next-generation sequencing, the genetic spectrum of POI has expanded significantly. To date, over 75 genes associated with POI have been identified, involving various processes, such as gonadal development, meiosis and DNA damage repair, follicular development, hormone metabolism, mitochondrial function, transcription factors, ligand receptors, apoptosis, and RNA metabolism.[27,28] This study demonstrates that *CKAP5*, a cytoskeletal protein gene, is a key contributor to the maintenance of ovarian reserve and oocyte development. CKAP5 regulates autophagy and DNA damage repair in the ovaries by modulating ATG7 and ATM. *CKAP5* haploinsufficiency impairs autophagic flux and DSBs repair, leading to a reduction in the primordial follicle pool, compromised oocyte quality, increased follicular apoptosis, and accelerated follicular atresia. A heterozygous variant in *CKAP5* (NM_0001008938.4, c.630 + 7_630 + 11delCAAAA) results in clinical POI in patients by disrupting CKAP5 protein function.

Meiosis is essential for forming haploid gametes and maintaining ovarian reserve. Only oogonia that enter meiosis develop into oocytes, which are surrounded by GCs to form primordial follicles, the basic functional units of the ovary.[29] Animal models with meiotic gene defects exhibit meiotic arrest, accumulation of DSBs, and oocyte apoptosis, ultimately resulting in a diminished ovarian reserve and reduced fertility phenotypes resembling human POI.[30] Dysfunction of these genes causes abnormal chromosome pairing, synapsis, and segregation in oocytes, as well as defects in homologous recombination repair and the production of aneuploid oocytes, contributing to unexplained infertility or early pregnancy loss.[30,31] POI caused by defects in meiotic genes such as *ATM* is classified as syndromic POI and is characterized by gonadal abnormalities, particularly hypoplasia with germ cell deficiencies.[32] In homozygous ATM-deficient mice, gametogenesis is severely disrupted as early as the leptotene stage of prophase I, leading to oocyte apoptotic degeneration and primordial follicle depletion.[24,33] Heterozygous ATM-deficient mice exhibit reduced primordial and primary follicles, prolonged oestrous cycles, and decreased ovarian function.[34] In oocytes, ATM-mediated DSBs repair preserves oocyte quality and viability. Knockdown of ATM in mouse oocytes increases sensitivity to DNA damage and apoptosis, leading to DSBs accumulation, preventing completion of the first meiotic division, and impairing blastocyst formation.[35] In addition, ATM plays a role in regulating the cell cycle checkpoint during the GV stage and in non-homologous end joining repair during the MII stage to preserve oocyte genomic stability.[36,37] Age-related declines in ATM function in oocytes are thought to be a major factor in oocyte ageing,[38] and GCs require ATM for DNA damage repair as they age.[39] Our study revealed that decreased CKAP5 expression leads to reduced ATM expression, impairing phosphorylation of downstream pathways, such as ATM-CHK2-P53 and ATM-SMC3/SMC1A, weakening DSBs repair capacity and resulting in γ-H2AX accumulation. Compared to $Ckap5^{+/+}$ mice, $Ckap5^{+/-}$ mice exhibited impaired DNA damage repair, particularly in oocytes and GCs, owing to ATM deficiency, hindering follicular self-repair and triggering apoptosis. Additionally, ROS accumulation in the GV-stage oocytes of $Ckap5^{+/-}$ mice further exacerbated DNA damage. As meiosis progresses, the co-localization of ATM and CKAP5 at the spindle suggests that CKAP5 deficiency intensifies meiotic arrest and hinders oocyte non-homologous end joining repair. Ultimately, this deficiency significantly compromises both the ovarian reserve and oocyte quality.

Autophagy governs follicular development, maintaining cellular and energy homoeostasis. Macroautophagy plays a crucial role in the survival of healthy primordial follicles. Adequate levels of autophagy prevent the accumulation of ROS in oocytes and maintain the protein levels of essential factors promoting oocyte development in the ovary, such as AMH, GDF9,

NOBOX, and TGFβ1.[40] When rapamycin inhibits the mammalian target of rapamycin (mTOR) pathway, increasing LC3B expression, inducing autophagy, and inhibiting apoptosis, it enhances the number of surviving oocytes.[41] In GCs, AMH inhibits FOXO3A phosphorylation in oocytes, thereby inducing ovarian autophagy, preventing excessive activation of primordial follicles, and protecting the ovarian reserve.[42] Ovarian ageing is associated with decreased expression of autophagy-related molecules.[43] Impaired autophagy is another recognized mechanism underlying POI. In the GCs of patients with biochemical POI, reduced LC3-II/I ratios and elevated P62 protein levels disrupt autophagic flux and hinder the degradation of WT1, resulting in hormonal secretion disorders.[44] Variants in autophagy-related genes, such as heterozygous ATG7 p.Phe403-Leu and ATG9A p.Arg758Cys, have been reported in patients with POI, with haploinsufficiency reducing cellular responses to starvation-induced autophagy.[45] As a critical regulatory gene for autophagy, ATG7 is essential for the maintenance of the ovarian reserve. Ovarian knockout of ATG7 leads to complete depletion,[23] whereas oocyte-specific ATG7 knockout results in partial loss of the primordial follicle pool,[46] accompanied by increased apoptosis in the ovaries of mice. In this study, in the case of *Ckap5* haploinsufficiency, ATG7 expression decreases but is not completely absent, which may result in a partial loss of the primordial follicle pool and follicle apoptosis, accounting for subfertility in *Ckap5*$^{+/-}$ mice.

Autophagy plays a crucial role in oocyte meiosis, helping to regulate oocyte quality with the assistance of GCs and ensuring normal follicular growth and ovulation. During the progression from primordial to mature Graafian follicles, LC3-II levels in oocytes increase by 20%–30%.[47] For mature oocytes arrested at MII post-ovulation, early activation of autophagy with rapamycin stabilizes intracellular Ca^{2+}, increases mitochondrial membrane potential, reduces ROS and active CASPASE-3 levels, and maintains the integrity of oocyte cortical granules and chromosomes/spindles, thereby preventing post-maturation oocyte ageing.[48] However, in ageing mice, the macroautophagy pathway is impaired in oocytes, with reduced autophagosomes and lysosomes.[49] Inhibition of oocyte autophagy leads to decreased mitochondrial membrane potential, excessive ROS production, DNA damage, and apoptosis, ultimately compromising the developmental potential.[50] Treatment with the autophagy activator rapamycin can alleviate these adverse effects, increase MII oocytes, improve IVF outcomes, enhance blastocyst formation rates, and reduce apoptosis.[51,52] Autophagy not only affects oocytes but also regulates GCs function. ATG7 and LC3II are highly expressed in human mature cumulus cells; when autophagy initiation is disrupted, pro-LC3 accumulates, leading to GCs death and reduced oocyte quality and female reproductive potential.[53] Disruption of GCs autophagy impairs tricarboxylic acid cycle homoeostasis, leading to abnormal mitochondrial distribution in oocytes, ROS accumulation, reduced nuclear maturation, and decreased embryo developmental competence.[54] In *Ckap5*$^{+/-}$ mice, autophagy in follicular cells is significantly impaired. The observed reduction in ATG7 and LC3 expression in *Ckap5*$^{+/-}$ mice mirrors the decline in CKAP5, with significant reductions in both oocytes and GCs. This suggests that CKAP5 deficiency impairs follicular growth and development by inhibiting autophagy, leading to apoptosis. This study shows that ATG7 and CKAP5 colocalize within the spindle region. CKAP5 deficiency not only reduced ATG7 expression in oocytes but also disrupted its localization in the spindle, potentially co-regulating spindle formation during oocyte nuclear maturation.

In addition to the reduction in oocyte quantity, a decline in oocyte quality poses a considerable challenge to fertility in patients with POI. In various animal models exhibiting POI characteristics, disruptions in the meiotic process and abnormal spindle structures have been observed, particularly in mice with homozygous deficiencies in genes such as *Dcaf13*,[55,56] *Esrp1*,[57] *Bnc1*,[58] and *Hfm1*.[59] Owing to ethical constraints and the limited availability of specimens, evidence substantiating oocyte meiotic maturation in patients with POI is scarce. Reports indicate that microinjection of human oocytes to reduce BNC1 expression leads to impaired first meiotic division and subsequent degradation of affected oocytes.[60] In this study, heterozygous *Ckap5*-deficient mice exhibited impaired oocyte maturation, meiotic arrest, and increased abnormal spindles, indicating compromised oocyte quality and accelerated ageing. However, note that not all animal models with abnormal oocyte nuclear maturation exhibit POI. The pathogenic mechanisms underlying the spindle abnormalities in ovarian insufficiency remain unclear. In patients with POI carrying a *CKAP5* variant, the reduction in ovarian reserve is accompanied by abnormalities in oocyte maturation and compromised oocyte quality, which may increase the likelihood of aneuploidy and miscarriage, further exacerbating fertility decline.[61]

The integrity of all structural domains of CKAP5 is essential for functional activity.[62] The heterozygous variant in *CKAP5* observed in patients with POI leads to protein truncation before the end of the first TOG domain, resulting in loss of function. This finding was consistent with the in vitro experimental results following *CKAP5* siRNA transfection, which demonstrated impaired autophagy and DNA damage repair. All patients with POI carrying the *CKAP5* variant presented with secondary amenorrhoea or menstrual irregularities. Although fertility potential has not yet been assessed in the two underage carriers (F1: III-5, aged 8 and F2: III-7, aged 16), continuous monitoring of ovarian function and fertility outcomes will be conducted.

We acknowledge several limitations in our study. Firstly, the limited availability and quality of human GC samples constrained the sample size for transcriptome analysis, potentially affecting statistical power and generalizability. To minimize confounding, we matched DOR patients and controls by age and BMI and excluded participants with smoking, drinking history, or chromosomal abnormalities. We then identified five candidate genes through transcriptome analysis and confirmed *CKAP5* as a potential pathogenic gene via gene burden analysis in POI and control cohorts. While this approach helps control for genetic background, we acknowledge that underlying genetic variations may still contribute to differential gene expression in the initial analysis. Additionally, some potential confounders, such as lifestyle factors (e.g., diet), were not fully addressed and may influence ovarian function.[63,64] We plan to incorporate these variables in future studies to strengthen our conclusions. Secondly, while our POI cohort provides valuable insights, its relatively small size and regional specificity may limit its representativeness, warranting validation in larger, more diverse cohorts. Finally, although we used a global heterozygous *Ckap5* knockout model, which has limitations in studying the ovarian-specific function of CKAP5, our data suggest that the observed phenotypic changes are primarily due to ovarian dysfunction. No significant systemic abnormalities, such as differences in body weight or organ morphology, were observed between the heterozygous knockout mice and wild-type controls, indicating that the effects are mainly ovarian-related. To address this limitation, future studies will employ conditional knockout models targeting *Ckap5* specifically in granulosa cells or oocytes. This cell-type-specific approach will allow us to more precisely investigate the ovarian function of CKAP5 and rule out any potential systemic effects, providing a clearer understanding of its role in ovarian ageing and pathology. These considerations highlight important avenues for future research, which we plan to explore in subsequent studies.

Our study suggests that CKAP5 maintains ovarian reserve and fertility by promoting autophagy and DNA damage repair. The heterozygous *CKAP5* variant (NM_0001008938.4, c.630 + 7_630 + 11delCAAAA) results in protein truncation and loss of function, ultimately leading to clinical POI. This study further extends the genotypic spectrum of POI and highlights the need for additional investigation into the function of *CKAP5* and its role in POI and other infertility disorders.

Contributors

ZH and JG were responsible for the experimental design and data interpretation. ZH, JG, RQ, FH, JZ and JJ performed the experiments. ZH, JG, RQ, FH, JZ, JJ, HX, JC and HH contributed reagents and interpreted the data. ZH, HH, HX and JC prepared the manuscript. ZH, HH, HX and JC verified the underlying data. All authors read and approved the final version of the manuscript.

Data sharing statement

All the data supporting the findings of this study are available within the article and Supplementary information files. RNA-seq information and raw data can be found in NCBI Bioproject numbers PRJNA1169996 and PRJNA1180492.

Declaration of interests

The authors declare no conflict of interest.

Acknowledgements

We thank all participants and their families, as well as the groups and physicians who supported this study. We thank all the doctors, nurses, and embryologists in the Reproductive Medicine Center of the Second Xiangya Hospital for their clinical work.

Appendix A. Supplementary data

Supplementary data related to this article can be found at https://doi.org/10.1016/j.ebiom.2025.105718.

References

1 Webber L, Davies M, Anderson R, et al, European Society for Human Reproduction and Embryology (ESHRE) Guideline Group on POI. ESHRE Guideline: management of women with premature ovarian insufficiency. *Hum Reprod*. 2016;31(5):926–937.
2 Golezar S, Ramezani Tehrani F, Khazaei S, Ebadi A, Keshavarz Z. The global prevalence of primary ovarian insufficiency and early menopause: a meta-analysis. *Climacteric*. 2019;22(4):403–411.
3 Ishizuka B. Current understanding of the etiology, symptomatology, and treatment options in premature ovarian insufficiency (POI). *Front Endocrinol (Lausanne)*. 2021;12:626924.
4 Jiao X, Ke H, Qin Y, Chen ZJ. Molecular genetics of premature ovarian insufficiency. *Trends Endocrinol Metab*. 2018;29(11):795–807.
5 Qin Y, Jiao X, Simpson JL, Chen ZJ. Genetics of primary ovarian insufficiency: new developments and opportunities. *Hum Reprod Update*. 2015;21(6):787–808.
6 Thawani A, Kadzik RS, Petry S. XMAP215 is a microtubule nucleation factor that functions synergistically with the gamma-tubulin ring complex. *Nat Cell Biol*. 2018;20(5):575–585.
7 Brouhard GJ, Stear JH, Noetzel TL, et al. XMAP215 is a processive microtubule polymerase. *Cell*. 2008;132(1):79–88.
8 Cassimeris L, Morabito J. TOGp, the human homolog of XMAP215/Dis1, is required for centrosome integrity, spindle pole organization, and bipolar spindle assembly. *Mol Biol Cell*. 2004;15(4):1580–1590.
9 Miller MP, Asbury CL, Biggins S. A TOG protein confers tension sensitivity to kinetochore-microtubule attachments. *Cell*. 2016;165(6):1428–1439.
10 Wu T, Dong J, Fu J, et al. The mechanism of acentrosomal spindle assembly in human oocytes. *Science*. 2022;378(6621):eabq7361.
11 Hu M, Yeh YH, Munakata Y, et al. PRC1-mediated epigenetic programming is required to generate the ovarian reserve. *Nat Commun*. 2022;13(1):4510.
12 Ge W, Wang JJ, Zhang RQ, et al. Dissecting the initiation of female meiosis in the mouse at single-cell resolution. *Cell Mol Life Sci*. 2021;78(2):695–713.
13 Wang JJ, Ge W, Zhai QY, et al. Single-cell transcriptome landscape of ovarian cells during primordial follicle assembly in mice. *PLoS Biol*. 2020;18(12):e3001025.
14 Lu A, Zhou CJ, Wang DH, et al. Cytoskeleton-associated protein 5 and clathrin heavy chain binding regulates spindle assembly in mouse oocytes. *Oncotarget*. 2017;8(11):17491–17503.
15 Practice Committee of the American Society for Reproductive M, Testing and interpreting measures of ovarian reserve: a committee opinion. *Fertil Steril*. 2020;114(6):1151–1157.
16 Long P, Wang L, Tan H, et al. Oligogenic basis of premature ovarian insufficiency: an observational study. *J Ovarian Res*. 2024;17(1):32.
17 Lv WQ, Lin X, Shen H, et al. Human gut microbiome impacts skeletal muscle mass via gut microbial synthesis of the short-chain fatty acid butyrate among healthy menopausal women. *J Cachexia Sarcopenia Muscle*. 2021;12(6):1860–1870.

18 Pedersen T, Peters H. Proposal for a classification of oocytes and follicles in the mouse ovary. *J Reprod Fertil*. 1968;17(3):555–557.
19 Wang F, Liu Y, Ni F, et al. BNC1 deficiency-triggered ferroptosis through the NF2-YAP pathway induces primary ovarian insufficiency. *Nat Commun*. 2022;13(1):5871.
20 Maggipinto MJ, Ford J, Le KH, et al. Conditional knockout of TOG results in CNS hypomyelination. *Glia*. 2017;65(3):489–501.
21 Isola JVV, Ocanas SR, Hubbart CR, et al. A single-cell atlas of the aging mouse ovary. *Nat Aging*. 2024;4(1):145–162.
22 Lopez-Otin C, Blasco MA, Partridge L, Serrano M, Kroemer G. Hallmarks of aging: an expanding universe. *Cell*. 2023;186(2):243–278.
23 Gawriluk TR, Hale AN, Flaws JA, Dillon CP, Green DR, Rucker EB 3rd. Autophagy is a cell survival program for female germ cells in the murine ovary. *Reproduction*. 2011;141(6):759–765.
24 Barlow C, Liyanage M, Moens PB, et al. Atm deficiency results in severe meiotic disruption as early as leptonema of prophase I. *Development*. 1998;125(20):4007–4017.
25 Lu H, Jing Y, Zhang C, et al. Aging hallmarks of the primate ovary revealed by spatiotemporal transcriptomics. *Protein Cell*. 2024;15(5):364–384.
26 Hansen KR, Hodnett GM, Knowlton N, Craig LB. Correlation of ovarian reserve tests with histologically determined primordial follicle number. *Fertil Steril*. 2011;95(1):170–175.
27 Franca MM, Mendonca BB. Genetics of primary ovarian insufficiency in the next-generation sequencing era. *J Endocr Soc*. 2020;4(2):bvz037.
28 Yang Q, Mumusoglu S, Qin Y, Sun Y, Hsueh AJ. A kaleidoscopic view of ovarian genes associated with premature ovarian insufficiency and senescence. *FASEB J*. 2021;35(8):e21753.
29 Pepling ME, Spradling AC. Mouse ovarian germ cell cysts undergo programmed breakdown to form primordial follicles. *Dev Biol*. 2001;234(2):339–351.
30 Huang C, Guo T, Qin Y. Meiotic recombination defects and premature ovarian insufficiency. *Front Cell Dev Biol*. 2021;9:652407.
31 Xie C, Wang W, Tu C, et al. Meiotic recombination: insights into its mechanisms and its role in human reproduction with a special focus on non-obstructive azoospermia. *Hum Reprod Update*. 2022;28(6):763–797.
32 Miller ME, Chatten J. Ovarian changes in ataxia telangiectasia. *Acta Paediatr Scand*. 1967;56(5):559–561.
33 Morita Y, Maravei DV, Bergeron L, et al. Caspase-2 deficiency prevents programmed germ cell death resulting from cytokine insufficiency but not meiotic defects caused by loss of ataxia telangiectasia-mutated (Atm) gene function. *Cell Death Differ*. 2001;8(6):614–620.
34 Clark KL, Keating AF. Ataxia-telangiectasia mutated coordinates the ovarian DNA repair and atresia-initiating response to phosphoramide mustard. *Biol Reprod*. 2020;102(1):248–260.
35 Suzuki R, Tan X, Szymanska KJ, et al. The role of declining ataxia-telangiectasia-mutated (ATM) function in oocyte aging. *Cell Death Discov*. 2024;10(1):302.
36 Marangos P, Carroll J. Oocytes progress beyond prophase in the presence of DNA damage. *Curr Biol*. 2012;22(11):989–994.
37 Martin JH, Bromfield EG, Aitken RJ, Lord T, Nixon B. Double strand break DNA repair occurs via non-homologous end-joining in mouse MII oocytes. *Sci Rep*. 2018;8(1):9685.
38 Titus S, Li F, Stobezki R, et al. Impairment of BRCA1-related DNA double-strand break repair leads to ovarian aging in mice and humans. *Sci Transl Med*. 2013;5(172):172ra121.
39 Sun XL, Jiang H, Han DX, et al. The activated DNA double-strand break repair pathway in cumulus cells from aging patients may be used as a convincing predictor of poor outcomes after in vitro fertilization-embryo transfer treatment. *PLoS One*. 2018;13(9):e0204524.
40 Zhihan T, Xinyi M, Qingying L, et al. Autophagy participates in cyst breakdown and primordial folliculogenesis by reducing reactive oxygen species levels in perinatal mouse ovaries. *J Cell Physiol*. 2019;234(5):6125–6135.
41 Sun YC, Wang YY, Sun XF, et al. The role of autophagy during murine primordial follicle assembly. *Aging (Albany NY)*. 2018;10(2):197–211.
42 Lecot-Connan T, Boumerdassi Y, Magnin F, et al. Anti-Müllerian hormone induces autophagy to preserve the primordial follicle pool in mice. *FASEB J*. 2024;38(5):e23506.
43 Li Q, Cai M, Wang J, et al. Decreased ovarian function and autophagy gene methylation in aging rats. *J Ovarian Res*. 2020;13(1):12.
44 Shao T, Ke H, Liu R, et al. Autophagy regulates differentiation of ovarian granulosa cells through degradation of WT1. *Autophagy*. 2022;18(8):1864–1878.
45 Delcour C, Amazit L, Patino LC, et al. ATG7 and ATG9A loss-of-function variants trigger autophagy impairment and ovarian failure. *Genet Med*. 2019;21(4):930–938.
46 Song ZH, Yu HY, Wang P, et al. Germ cell-specific Atg7 knockout results in primary ovarian insufficiency in female mice. *Cell Death Dis*. 2015;6(1):e1589.
47 Leopardo NP, Velazquez ME, Cortasa S, Gonzalez CR, Vitullo AD. A dual death/survival role of autophagy in the adult ovary of Lagostomus maximus (Mammalia- Rodentia). *PLoS One*. 2020;15(5):e0232819.
48 Lin FH, Zhang WL, Li H, et al. Role of autophagy in modulating post-maturation aging of mouse oocytes. *Cell Death Dis*. 2018;9(3):308.
49 Peters AE, Caban SJ, McLaughlin EA, et al. The impact of aging on macroautophagy in the pre-ovulatory mouse oocyte. *Front Cell Dev Biol*. 2021;9:691826.
50 Shen XH, Jin YX, Liang S, et al. Autophagy is required for proper meiosis of porcine oocytes maturing in vitro. *Sci Rep*. 2018;8(1):12581.
51 Song BS, Kim JS, Kim YH, et al. Induction of autophagy during in vitro maturation improves the nuclear and cytoplasmic maturation of porcine oocytes. *Reprod Fertil Dev*. 2014;26(7):974–981.
52 Li J, Balboula AZ, Aboelenain M, et al. Effect of autophagy induction and cathepsin B inhibition on developmental competence of poor quality bovine oocytes. *J Reprod Dev*. 2020;66(1):83–91.
53 Kang W, Ishida E, Yamatoya K, et al. Autophagy-disrupted LC3 abundance leads to death of supporting cells of human oocytes. *Biochem Biophys Rep*. 2018;15:107–114.
54 He H, Wang J, Mou X, et al. Selective autophagic degradation of ACLY (ATP citrate lyase) maintains citrate homeostasis and promotes oocyte maturation. *Autophagy*. 2023;19(1):163–179.
55 Zhang J, Zhang YL, Zhao LW, et al. Mammalian nucleolar protein DCAF13 is essential for ovarian follicle maintenance and oocyte growth by mediating rRNA processing. *Cell Death Differ*. 2019;26(7):1251–1266.
56 Zhang J, Zhang YL, Zhao LW, et al. The CRL4-DCAF13 ubiquitin E3 ligase supports oocyte meiotic resumption by targeting PTEN degradation. *Cell Mol Life Sci*. 2020;77(11):2181–2197.
57 Yu L, Zhang H, Guan X, Qin D, Zhou J, Wu X. Loss of ESRP1 blocks mouse oocyte development and leads to female infertility. *Development*. 2021;148(2).
58 Ma J, Zeng F, Schultz RM, Tseng H. Basonuclin: a novel mammalian maternal-effect gene. *Development*. 2006;133(10):2053–2062.
59 Wang H, Zhong C, Yang R, et al. Hfm1 participates in Golgi-associated spindle assembly and division in mouse oocyte meiosis. *Cell Death Dis*. 2020;11(6):490.
60 Zhang D, Liu Y, Zhang Z, et al. Basonuclin 1 deficiency is a cause of primary ovarian insufficiency. *Hum Mol Genet*. 2018;27(21):3787–3800.
61 Tilia L, Chapman M, Kilani S, Cooke S, Venetis C. Oocyte meiotic spindle morphology is a predictive marker of blastocyst ploidy-a prospective cohort study. *Fertil Steril*. 2020;113(1):105–113.
62 Slater PG, Cammarata GM, Samuelson AG, Magee A, Hu Y, Lowery LA. XMAP215 promotes microtubule-F-actin interactions to regulate growth cone microtubules during axon guidance in Xenopuslaevis. *J Cell Sci*. 2019;132(9).
63 Guo X, Zhu Y, Guo L, et al. BCAA insufficiency leads to premature ovarian insufficiency via ceramide-induced elevation of ROS. *EMBO Mol Med*. 2023;15(4):e17450.
64 Shelling AN, Ahmed Nasef N. The role of lifestyle and dietary factors in the development of premature ovarian insufficiency. *Antioxidants (Basel)*. 2023;12(8):1601.